Article

Not peer-reviewed version

# Combining a Drug and a Nutraceutical: A New Cocrystal of Praziquantel and Curcumin

Camila Caro Garrido *, Marie Vandooren, Koen Robeyns, Damien P. Debecker, Patricia Luis Alconero, Tom Leyssens *

Posted Date: 8 January 2024

doi: 10.20944/preprints202401.0598.v1

Keywords: Praziquantel, Curcumin, Nutraceutical, Coformer, Cocrystal Solvate, Cocrystal

*Article*

# Combining a Drug and a Nutraceutical: A New Cocrystal of Praziquantel and Curcumin

**Camila Caro Garrido [1,*], Marie Vandooren [1], Koen Robeyns [1], Damien P. Debecker [1], Patricia Luis [2], and Tom Leyssens [1,*]**

[1] Institute of Condensed Matter and Nanosciences, UCLouvain, 1 Place Louis Paster, B-1348 Louvain-la-Neuve, Belgium; marie.vandooren@student.uclouvain.be (M.V.); koen.robeyns@uclouvain.be (K.R); Damien.debecker@uclouvain.be (D.P.D.)

[2] Institute of Mechanics, Materials and Civil Engineering, UCLouvain, 2 Place Sainte Barbe, B-1348 Louvain-la-Neuve, Belgium: patricia.luis@uclouvain.be

* Correspondence: camila.carogarrido@uclouvain.be (C.C.G.); tom.leyssens@uclouvain.be (T.L.); Tel: +32-497881129 (C.C.G.); +32-10472811 (T.L)

**Abstract:** This study explores the cocrystallization between the drug praziquantel (PZQ) and the nutraceutical curcumin (CU). The investigation revealed two novel solid forms: a cocrystal solvate with ethyl acetate and a non-solvated cocrystal. This novel drug-nutraceutical cocrystal is identified as "generally recognized as safe" (GRAS) praziquantel-curcumin-ethyl acetate (2:1:1) cocrystal solvate. This latter undergoes desolvation, leading to the formation of the praziquantel-curcumin (2:1) cocrystal. The cocrystal solvate has ethyl acetate molecules occupying the voids with minimal interactions within the crystal lattice. The application of heat treatment induces solvent removal and prompts the transition to the non-solvated cocrystal, as highlighted by VT-XRD. Thermal analyses demonstrate the stability of the cocrystal solvate up to approximately 100°C, beyond which it transforms into the non-solvated phase, which eventually melts at 130°C. Representation of praziquantel (PZQ) and curcumin (CU) cocrystallizations.

**Keywords:** Praziquantel, Curcumin, Nutraceutical, Coformer, Cocrystal Solvate, Cocrystal

## 1. Introduction

Praziquantel (PZQ) marketed as [Pr]BILTRICIDE® by Bayer is an acylated quinoline-pyrazine derivative (Figure 2). It is the most effective and widely administered first-line and broad-spectrum anthelmintic drug in both humans and animals. This medicine is used against all *Schistosoma* spp. for control and (preventive) treatment [1]. Schistosomiasis, or bilharzia, is an acute and chronic water-based disease caused by parasitic trematode flatworms [2]. This tropical disease has considerable morbidity worldwide, particularly in sub-Saharan Africa, and school-aged children (aged 5 to 14 years) are recognized as especially vulnerable to this infection [3]. Human beings are contaminated by infested water during routine actions such as domestic, occupational, agricultural, and recreational activities. This disease essentially affects populations that do not have access to potable water. In 2021, more than 250 million people needed preventive treatment [4]. This explains why PZQ is enlisted in the World Health Organization's (WHO) Model List of Essential Medicines [5].

Preprints (www.preprints.org) | NOT PEER-REVIEWED | Posted: 8 January 2024 doi:10.20944/preprints202401.0598.v1



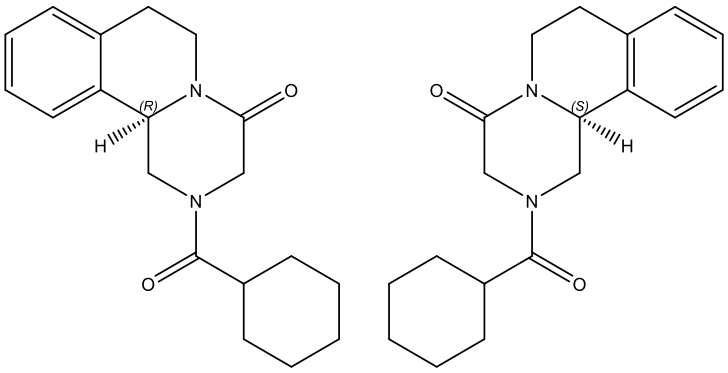


**Figure 1.** Molecular structures of R- and S-PZQ enantiomers.

Praziquantel is a chiral compound and is commercially marketed as a racemate (RS-PZQ). However, the schistosomicidal activity mainly comes from the (R)-enantiomer (R-PZQ) [6]. This means that only half of the administered drug contributes to the therapeutic activity. Besides, the (S)-enantiomer (S-PZQ) is responsible for the bitter taste of praziquantel [7]. Furthermore, RS-PZQ exhibits poor solubility in aqueous media (0.40 mg/mL in water at 25°C) and consequently shows poor bioavailability, imposing the requirement for high clinical doses (large tablets of 600 mg) [8]. The tablet's dimension and the unpleasant taste of praziquantel, even as a syrup or crushed and mixed with juice, are challenging for children, who form the largest patient group [9].

A common approach in crystal engineering to enhance API properties, such as low water solubility, low dissolution rate, or low chemical stability, is to screen for alternative solid forms, such as amorphous phases [10], polymorphs [11], salts [12], and/or cocrystals [13], all showing a variation in lattice energy and hence pharmaceutical properties. The search for new solid forms capable of improving solubility and consequently reducing high dosages is relevant in the case of praziquantel. Since PZQ has no ionizable group, it is unsuitable for salt formation. It does, however, feature two carbonyl groups capable of functioning as hydrogen bond acceptors, making them excellent candidates for cocrystal formation [14]. To date, 3 polymorphs [14–16], 3 solvates [17, 18], and 31 cocrystals [14, 19–23] of RS-PZQ have been reported in the CCDC (Cambridge Crystallographic Data Center) database. Based on the analysis of these structures, RS-PZQ has been reported as an ideal coformer (CCF) for cocrystal formation with carboxylic acids (e.g., oxalic acid, malonic acid, malic acid, etc.) or compounds containing polyphenol hydroxyl groups (e.g., ferulic acid, kaempferol, quercetin, etc.) [24]. We, therefore, selected curcumin (CU), a well-studied natural polyphenol and a nutraceutical with a ginger-like taste, as a potential cocrystal former for RS-PZQ. This coformer can potentially alleviate the bitterness of praziquantel.

Curcumin (Figure 2) is an intense yellow-orange polyphenolic pigment extracted from the turmeric rhizome, belonging to the ginger family. This bioactive molecule is also known as food additive E100 and has numerous applications as a flavoring agent, coloring agent, food preservative, and dietary supplement [25]. It is also considered a nutraceutical, a substance of natural origin that extends its usefulness beyond basic nutritional functions [26]. Curcumin is the main pharmacologically active constituent of turmeric among curcuminoids (demethoxycurcumin, bisdemethoxycurcumin, etc.) [27]. It is used in traditional medicine and is claimed to have many pharmacological effects (such as antioxidant, anti-inflammatory, antimicrobial, etc.) [28, 29]. Curcumin shows keto-enol tautomerism and can interact with various targets (protein kinases, transcription factors, etc.) [30]. Despite being a GRAS (Generally Recognized as Safe) compound, it has very poor aqueous solubility (0.6 μg/mL in pure water at RT) and low bioavailability, limiting its therapeutic effectiveness [31]. Previous studies have shown curcumin to cocrystallize with coformers such as resorcinol, pyrogallol, cinnamic acid, resveratrol, salicylic acid, and hydroxyquinol [32–35].

Here, we aimed at enhancing RS-PZQ properties by forming a new drug-nutraceutical cocrystal [36, 37] with curcumin. Such a cocrystal could potentially reduce the bitter taste of praziquantel tablets, enhance the solubility and bioavailability of curcumin as well as some of the adverse effects of the drug (headache, abdominal pain, muscle pain, fatigue, and weakness) [1, 9].

Preprints (www.preprints.org) | NOT PEER-REVIEWED | Posted: 8 January 2024 doi:10.20944/preprints202401.0598.v1



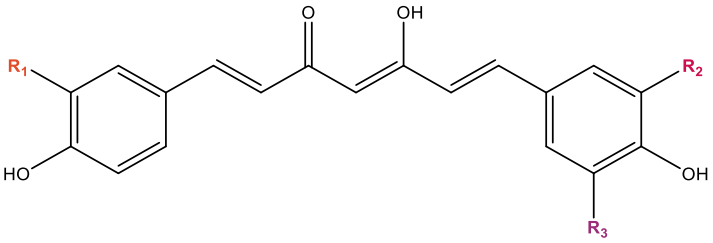


Curcumin (CU): $R_1$ = -$OCH_3$, $R_2$ = -$OCH_3$, $R_3$ = -H
Demethoxycurcumin (DMC): $R_1$ = -H, $R_2$ = -H, $R_3$ = -$OCH_3$
Bis(demethoxy)curcumin (BDMC): $R_1$ = -H, $R_2$ = -H, $R_3$ = -H

**Figure 2.** Molecular structures of turmeric main curcuminoids, represented as enol forms.

## 2. Materials and Methods

### *2.1. Materials*

Natural extracted powder of curcumin was purchased from Lesen Xi'an Le Sen Bio-technology Co., Ltd. (Phytochem & Herbs Extracts Solutions Provider) (Xi'an, China). This powder contains curcuminoids such as curcumin, demethoxycurcumin and bis(dimethoxy)curcumin. Synthetic curcumin (CAS: 458-37-7, > 97.0 %) and racemic praziquantel (CAS: 55268-74-1, > 98.0 %) were acquired from TCI EUROPE N.V. (Zwijndrecht, Belgium). Solvents were acquired from VWR International BV (Brecht, Belgium). All materials were used as received without any further purification.

### *2.2. Cocrystal screening by liquid-assisted grinding (LAG) experiments*

Screening of cocrystals between natural extracted powder of curcumin and racemic praziquantel was performed by liquid-assisted grinding (LAG) in the MM 400 Mixer Mill grinder manufactured by RETSCH (Haan, Germany). The latter is equipped with two grinding jars that can each contain 5 Eppendorf tubes of 2 mL. Each tube was filled with an equimolar quantity (0.4 mmol) of curcumin and racemic praziquantel, 100 µL of toluene as well as 4 small stainless-steel beads (Ø 3 mm). The grinding program was set for 90 minutes at a beating frequency of 30 Hz. The resulting ground powders were studied by X-ray powder diffraction (XRPD).

### *2.3. Congruency experiments*

Congruency experiments were carried out by slurry crystallization. At first, slurry experiments were prepared by suspending an equimolar amount (0.3 mmol) of racemic praziquantel and natural extracted powder of curcumin in a suitable amount of solvent (from 1 to 4 mL). The solvents tested include 2-propanol (IPA), acetonitrile (ACN), ethanol (EtOH), ethyl acetate (EtOAc), and methanol (MeOH). The suspensions were shaken at 150 rpm for 3 to 4 days at room temperature (RT) in 5 mL sealed vials by the "Orbital Shaker SO3" from Stuart Scientific. The powders were then filtered, washed with fresh solvent, dried and analyzed by X-ray powder diffraction.

Then, slurry experiments were carried out using a 2:1 ratio of racemic praziquantel (0.6 mmol) and synthetic curcumin (0.3 mmol) in a suitable amount of ethyl acetate (from 1 to 4 mL). The suspensions were also shaken at 150 rpm for 3 to 4 days at RT in 5 mL sealed vials by the "Orbital Shaker SO3" from Stuart Scientific. The powders were then filtered, washed with fresh ethyl acetate, dried and analyzed by XRPD.

### *2.4. Single crystal growth*

Single crystals were grown by slow evaporation and cooling of the supernatants retrieved from the slurry experiments (prepared as previously described using a 2:1 ratio of racemic praziquantel and synthetic curcumin in EtOAc). Concerning the slow evaporation experiments, supernatants were left to evaporate slowly throughout 3 to 10 days at +/- RT. For the single crystals formed by cooling,

 doi:10.20944/preprints202401.0598.v1



supernatants retrieved from the slurry experiments were placed in a refrigerator at -4 °C. Suitable crystals of the 2:1: praziquantel-curcumin-ethyl acetate cocrystal solvate were successfully obtained both from cooling as well as slow evaporation experiments.

*2.5. X-ray powder diffraction (XRPD)*

X-ray diffraction measurements were carried out using a Siemens D5000 diffractometer, furnished with a Cu cathode (with a wavelength of $\lambda$ = 1.5418 Å) running at 40 kV and 40 mA and employing a Bragg-Brentano geometry. X-ray patterns were recorded in 2θ angle values, in the scanning range from 5 to 35°, with a step size of 0.02° and an integration time of 2 s (rate of 0.6°. min$^{-1}$). Patterns of known starting compounds were simulated from the single crystal structures using Mercury 4.2.0 software [38]. The obtained X-ray diffraction patterns were analyzed using WinPLOTR software [39].

*2.6. Single crystal X-ray diffraction analysis (SCXRD)*

Single crystal X-ray diffraction data were collected on a MAR345 image plate detector using Mo K$\alpha$ radiation from an Incoatec microfocus source (Montel mirrors). CrysAlis$^{PRO}$ software was used to integrate the images, and the implemented absorption correction was applied [40]. Structure resolution was carried out by dual space direct methods (SHELXT) [41], and the structure was then refined against $F^2$ using SHELX-2018/3 [42]. PLATON allowed the symmetry analysis and validation of the structure [43]. Figures were made using the molecular visualization software Mercury 4.2.0 [38].

To obtain (non-solvated) 2:1 praziquantel-curcumin cocrystals, a single crystal of 2:1:1 praziquantel-curcumin-ethyl acetate cocrystal solvate was mounted in a glass capillary and placed in an $N_2$-flow of an Oxford Cryostream set at RT. The system was heated from RT to 370 K at 3°C/min, then further from 370 K to 390 K at 2°C/min. Unit cell determination was performed at 380 K and 390 K to follow the crystal-to-crystal transformation. Finally, the crystal inside the capillary was cooled down to 298 K at 4°C/min. SCXRD data were collected on the crystal inside the capillary and treated as previously described.

*2.7. Variable temperature X-ray diffraction (VT-XRD)*

XRPD patterns were measured in glass capillaries with a diameter of 0.7 mm (Hilgenberg GmbH). The analysis used a MAR345 image plate detector (sample-detector distance, 200 mm) and a microfocus Incoatec Source (IμS) Mo (Montel mirror) source operating at 50 kV and 600 μA. The sample was exposed for 5 min while the capillary containing the sample was rotated by 180°. Diffraction data were integrated using Fit2D software (with data obtained from a 0.1 mm-diameter capillary filled with LaB6 as a calibrant). For variable-temperature X-ray powder diffraction, the sample-filled capillary was heated using a Cryostream 800PLUS.

A capillary filled with the cocrystal solvate was heated at 3 K.min$^{-1}$ to 380 K. The sample was allowed to equilibrate for a few minutes, and an XRD pattern was recorded. Subsequent PXRD patterns were recorded after 2 K.min$^{-1}$ heating ramps at 385 and 395 K.

*2.8. Thermogravimetric analysis (TGA)*

TGA measurements were carried out using a Mettler Toledo TGA-STDA 851e. Approximately 5 to 10 mg of sample were placed in an aluminum oxide crucible, and the temperature was ramped from 25 °C to 600 °C at a heating rate of 5 °C.min$^{-1}$. The purge gas was nitrogen, with a continuous flow rate of 50 mL.min$^{-1}$. The data were treated with the STARe 12.12 software.

*2.9. Differential scanning calorimetry (DSC) analysis*

Differential scanning calorimetry measurements were conducted using a TA DSC2500. A sample mass of approximately 5 to 10 mg was placed in an aluminum Tzero pan with a perforated hermetic lid, and the temperature was scanned at a rate of 5 °C.min$^{-1}$: first heating from 25 °C to 150 °C, then

Preprints (www.preprints.org) | NOT PEER-REVIEWED | Posted: 8 January 2024 doi:10.20944/preprints202401.0598.v1



cooling from 150 °C to 25 °C, to eventually finish the cycle with a second heating from 25 to 220 °C. The purge gas was nitrogen, with a continuous flow rate of 50 mL.min$^{-1}$. The data were treated with the TA Instruments Trios V5.1.1.46572 software.

*2.10. Proton nuclear magnetic resonance ($^1$H NMR)*

Proton nuclear magnetic resonance spectra were recorded on a Bruker 300 MHz spectrometer. The powders obtained from the slurry experiments were solubilized in DMSO-d$^6$. $^1$H NMR chemical shifts are reported in parts per million (ppm) relative to the chemical shift of the peak of the deuterated solvent used ($(CD_3)_2SO$; 2.50 ppm). Spectral multiplicities are noted as follows: singlet = s, doublet = d, triplet = t, quartet = q and multiplet = m.

## 3. Results and discussion

*3.1. Cocrystal identification*

Praziquantel has two amide groups that have the capacity to establish robust hydrogen bonding interactions. We have opted for curcumin (CU), a well-studied natural polyphenol, as our choice for generating cocrystals with racemic praziquantel. The selection of curcumin is motivated by its potential to form non-covalent intermolecular interactions, particularly hydrogen bonds, thus potentially facilitating the creation of supramolecular synthons.

Screening experiments were conducted to search for new cocrystalline phases of racemic praziquantel using the liquid-assisted grinding method. A potential novel solid phase was identified through X-ray powder diffraction analysis (Figure 3). Comparison of the XRPD patterns of racemic praziquantel, curcumin, and the solid obtained from the toluene LAG experiment indicates that CU and RS-PZQ generated a new solid form significantly different from the known forms of the starting materials. However, the diffractogram of the solids resulting from the LAG experiment shows peaks of unreacted curcumin, suggesting that a new potential solid form exists in a ratio other than a 1:1 ratio.

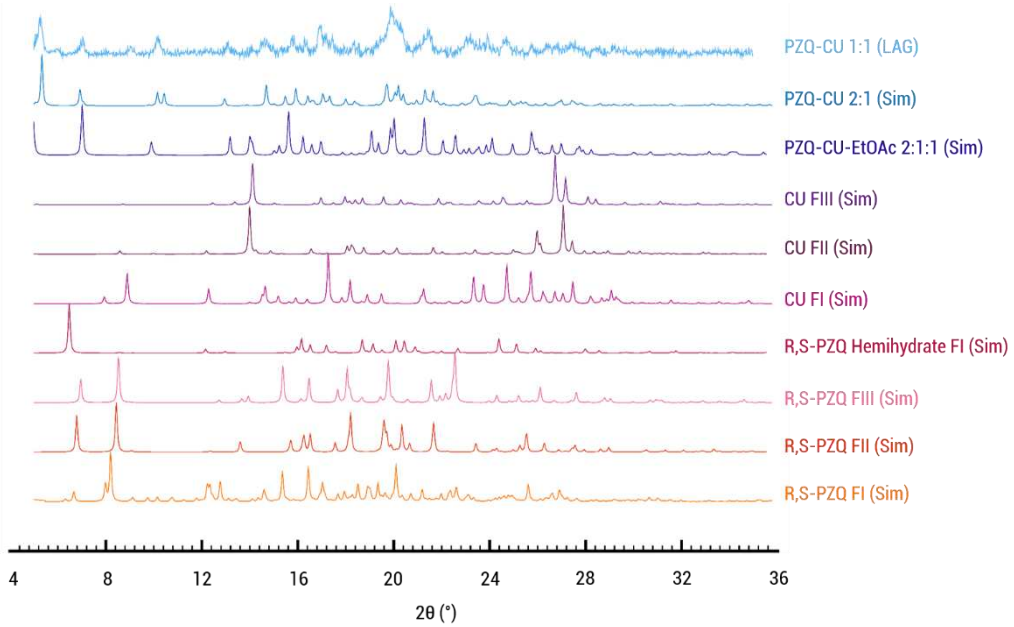


**Figure 3.** Normalized diffraction patterns. Simulated diffraction pattern of the known polymorphs (FI-III) and hemihydrate of the parent compounds racemic praziquantel and curcumin, praziquantel-curcumin-ethyl acetate cocrystal solvate (PZQ-CU-EtOAc 2:1:1) and praziquantel-curcumin cocrystal (PZQ-CU 2:1), and experimental patterns of the powder obtained by toluene LAG.

1:1 slurry experiments were performed in isopropanol, acetonitrile, ethanol, methanol, and ethyl acetate (EtOAc). For all but this latter, curcumin was obtained in suspension (Figure S1). The slurry

 doi:10.20944/preprints202401.0598.v1



from ethyl acetate shows a pattern different from the parent compounds (Figure S1). Single crystals were therefore sought using this solvent in a 1:1, 2:1, and 1:2 ratio. The 2:1 ratio led to the formation of a praziquantel-curcumin-ethyl acetate cocrystal solvate (PZQ-CU-EtOAc 2:1:1). As will be shown later on, this phase can be desolvated, leading to the praziquantel-curcumin cocrystal (PZQ-CU 2:1), also identified during the toluene LAG experiment (Figure 3).

The main crystallographic parameters are compared in Table 1, with a detailed discussion of each solid form provided below. Complete crystallographic data can be found in the Supporting Information (SI), specifically in Table S1. Additionally, PZQ-CU-EtOAc 2:1:1 cocrystal solvate SCXRD was also measured at RT (Table S2).

**Table 1.** Main crystallographic parameters of the praziquantel-curcumin-ethyl acetate (2:1:1) cocrystal solvate and the praziquantel-curcumin (2:1) cocrystal.

| | **PZQ-CU-EtOAc (2:1:1)** | **PZQ-CU (2:1)** |
|---|---|---|
| **Formula** | $C_{21}H_{20}O_6$,·2($C_{19}H_{24}N_2O_2$), ·$C_4H_8O_2$ | $C_{21}H_{20}O_6$,·2($C_{19}H_{24}N_2O_2$) |
| **MW (g.mol$^{-1}$)** | 1081.30 | 993.20 |
| **T (K)** | 150 | RT |
| **Crystal system** | Monoclinic | Monoclinic |
| **Space group** | *C*2/*c* | $P2_1/n$ |
| **a, b, and c (Å)** | 37.992(3), 5.9769(5), 26.8477(15) | 27.330(4), 5.8708(7), 35.486(7) |
| **$\alpha$, $\beta$, and $\gamma$ (°)** | 90, 110.218(7), 90 | 90, 111.06(2), 90 |
| **Cell volume (Å$^3$)** | 5720.79 | 5313.4 |
| **Z** | 4 | 4 |

*3.2. Structural and thermal characterization*

As shown in Table 1, PZQ-CU-EtOAc (2:1:1) crystallizes in the C-centered monoclinic space group *C*2/*c* and comprises four molecules within its unit cell. It presents itself as a stoichiometric solvate. Ethyl acetate molecules exhibit limited interactions within the crystal lattice; they primarily occupy the voids in the structure and exert minimal influence on its packing arrangement, as shown in Figure 4. Furthermore, these solvent molecules are found disordered on an inversion center and lack stabilization interactions. PZQ molecules have adopted an *anti*-conformation of the C=O groups of the piperazinone-cyclohexylcarbonyl segment. Curcumin molecules are located on a 2-fold axis and show whole-molecule disorder (91/9 ratio for the structure determined at 150 K, 85/15 ratio for the structure determined at RT) within the crystal lattice and present strong intramolecular O-H—O=C hydrogen bonds involving the enol group, which is preserved for the disordered molecules. This hydrogen bond has an $S_1^1(6)$ intramolecular hydrogen bond pattern, according to Etter's graph-set notation [44] (following descriptor *a* in Figure 4). Praziquantel and curcumin molecules are linked by two hydrogen bonds, giving a molecular assembly of the composition PZQ–CU–PZQ. These latter interactions result in two $D_1^1(2)$ finite patterns coupled into one $D_2^2(21)$ finite pattern, involving the -OH group of curcumin and the C=O function of the cyclohexylcarbonyl group of praziquantel, following the *b* descriptor through the < *b* > *b* path.

Preprints (www.preprints.org) | NOT PEER-REVIEWED | Posted: 8 January 2024 doi:10.20944/preprints202401.0598.v1



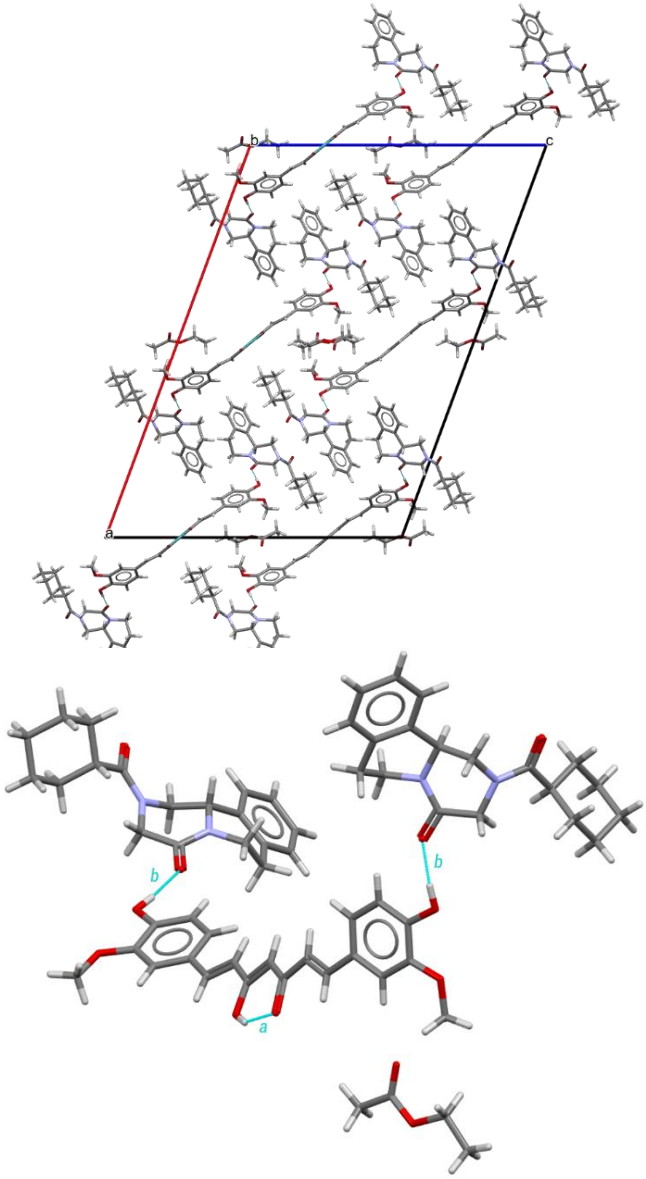


**Figure 4.** Structure of the PZQ-CU-EtOAc (2:1:1) cocrystal solvate. On the left: crystal packing, viewed along the b-axis; on the right: hydrogen bond arrangement, viewed along the origin. The structure is represented without disorder for more clarity.

Bulk material of the cocrystal solvate can be obtained from a 2:1 slurry experiment in ethyl acetate at room temperature (see Supporting Information, Figure S1). $^{1}$H NMR analysis (see Supporting Information, Figure S3) confirms the 2:1:1 stoichiometry of this novel cocrystal solvate composed of praziquantel, curcumin, and ethyl acetate.

Due to the loosely bound ethyl acetate molecules, the cocrystal solvate can be desolvated in a single-crystal to single-crystal transition. The **Praziquantel-curcumin (2:1) cocrystal** structure was thus obtained by slowly heating a single crystal from RT to 370 K at 3 °C/min, then at a slower heating rate of 2 °C/min from 370 K to 390 K, and finally cooling down to 298 K at 4 °C/min. PZQ-CU (2:1) is shown to crystallize in the primitive monoclinic space group $P2_1/n$ and contains four molecules per unit cell. The comparison of the unit cell parameters of the cocrystal solvate and the cocrystal in Table 1 shows these two solid forms to be only slightly different, leading to only slightly distinct XRPD patterns (Figure 3). The crystal lattices indeed exhibit a high degree of similarity (Figure 5), with the solvent removal leading to a slight crystal lattice volume reduction.

Preprints (www.preprints.org) | NOT PEER-REVIEWED | Posted: 8 January 2024 doi:10.20944/preprints202401.0598.v1



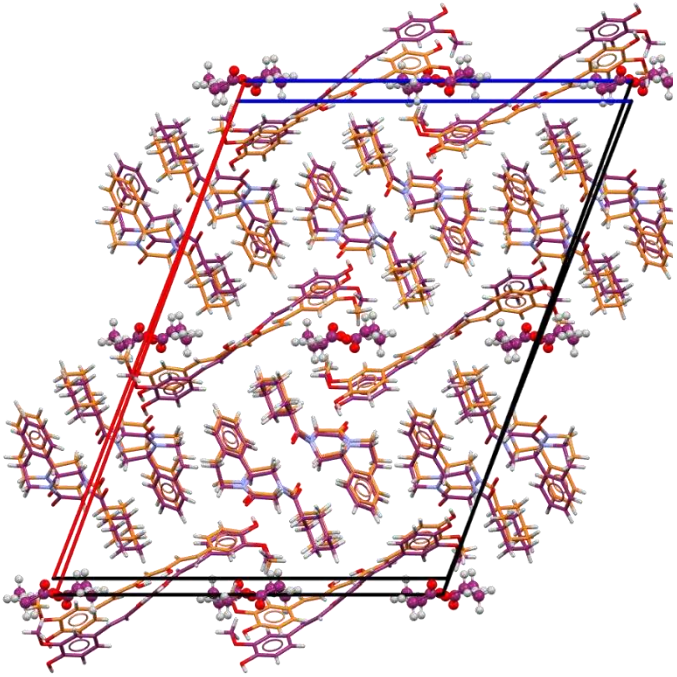

**Figure 5.** Packing superposition of the 2:1:1 PZQ-CU-EtOAc cocrystal solvate (carbon atoms in dark purple) and the 2:1 PZQ-CU cocrystal (carbon atoms in orange), viewed along the b-axis (without the disorder).

In the praziquantel-curcumin (2:1) cocrystal, the dominant supramolecular interactions are therefore similar to the ones in the cocrystal solvate, as shown in Figure 6 and Table 3. Curcumin molecules form strong intramolecular O-H--O hydrogen bonds following an $S_1^1(6)$ intramolecular hydrogen bond pattern. Two R- (or two S-) praziquantel molecules are connected to 1 curcumin by two hydrogen bonds, combined in two $D_1^1(2)$ finite patterns merged into one $D_2^2(21)$ finite pattern. The molecular assembly PZQ-CU-PZQ involves the hydroxy group of curcumin and the carbonyl function of the cyclohexylcarbonyl group of praziquantel, following the *b* and *c* descriptors along the $< b > c$ path.

Preprints (www.preprints.org) | NOT PEER-REVIEWED | Posted: 8 January 2024 doi:10.20944/preprints202401.0598.v1



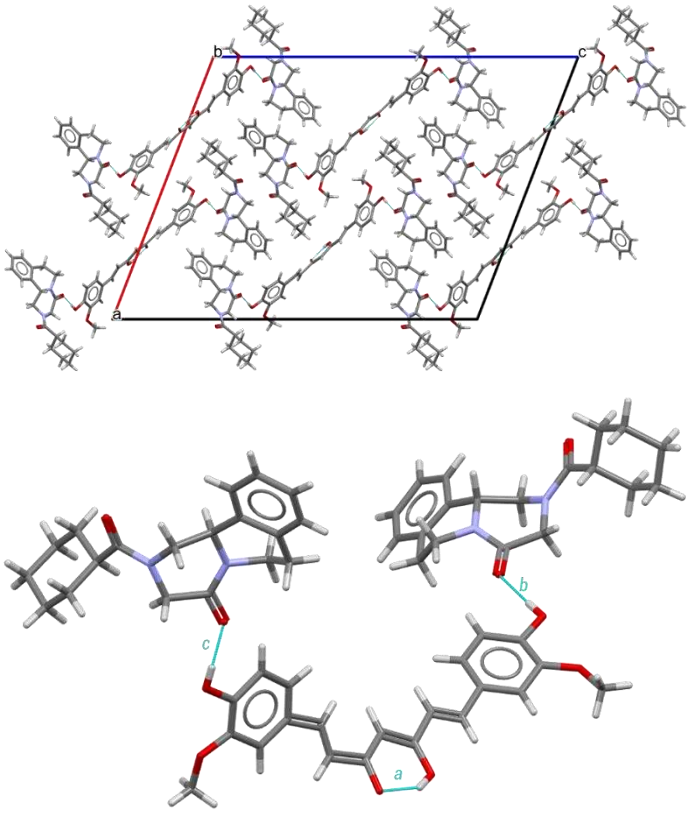


**Figure 6.** Structure of the PZQ-CU (2:1) cocrystal. Top: crystal packing, viewed along the b-axis; bottom: hydrogen bond arrangement.

As shown in Figure 3, the simulated XRPD pattern of the praziquantel-curcumin (2:1) cocrystal closely matches the experimental pattern obtained by liquid-assisted grinding with toluene, with the experimental pattern showing some parent compound remaining.

Thermogravimetric analysis (Figure 7) shows the praziquantel-curcumin-ethyl acetate (2:1:1) cocrystal solvate to be stable up to approximately 100 °C, at which point a weight loss of 7 % is observed, which closely aligns with the theoretically expected weight loss of a single ethyl acetate molecule from the cocrystal solvate (theoretical value of 8.15 %). The DSC analysis conducted using a heating rate of 5 °C.min$^{-1}$ (Figure 8) also shows this desolvation as an endothermic peak with $T_{onset}$ = 101.90 °C ($T_{peak}$ = 113.32 °C) and a heat of desolvation of ΔH = 44 j.g$^{-1}$. X-ray powder diffraction (XRPD) analysis of the resulting powder (see Supporting Information, Figure S2) confirms the presence of PZQ-CU (2:1) cocrystal as the residual phase, validating the desolvation process. The melting point of PZQ-CU (2:1) cocrystal is found at $T_{onset}$ = 129.51 °C, which is notably lower than the individual melting points of the parent compounds ($T_{melting}$ = 183 °C for curcumin; $T_{melting}$ = 136 °C for praziquantel). Degradation of the resulting melt occurs at approximately 190°C. Upon cooling the melt and reheating, a glass transition occurs at $T_{midpoint}$ = 53.15°C. No (re)crystallization peaks were observed during the temperature cycling.

Preprints (www.preprints.org) | NOT PEER-REVIEWED | Posted: 8 January 2024 doi:10.20944/preprints202401.0598.v1



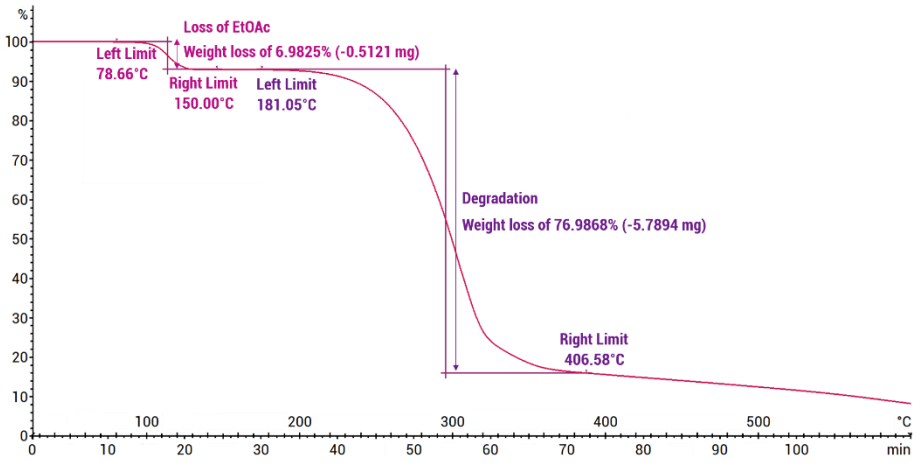


**Figure 7.** Thermogravimetric analysis of PZQ-CU-EtOAc (2:1:1) cocrystal solvate obtained by slurry in ethyl acetate (initial sample mass: 7.5200 mg), expressed in weight loss (%) as a function of temperature (°C) and time (min).

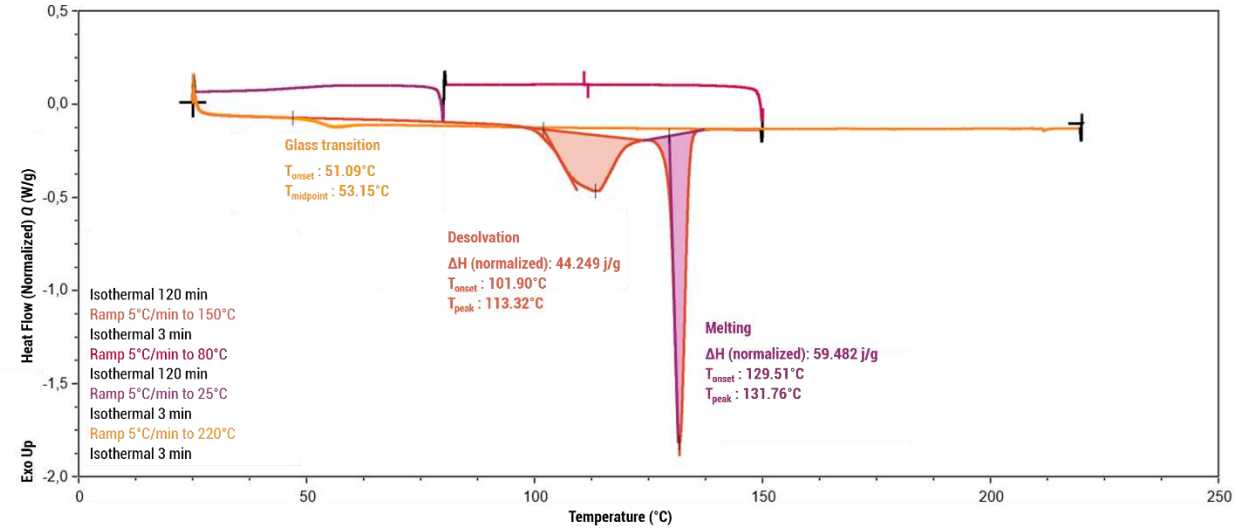


**Figure 8.** Differential scanning calorimetry analysis of PZQ-CU-EtOAc (2:1:1) cocrystal solvate obtained by slurry in ethyl acetate, expressed in mW as a function of temperature (°C) and time (min).

Furthermore, variable-temperature X-ray diffraction (VT-XRD) experiments were performed between RT and 121.85 °C (395 K), revealing the gradual change from the (2:1:1) cocrystal solvate to the desolvated (2:1) cocrystal, providing valuable insight into thermal behaviors and phase evolution. Figure 9 illustrates that the simulated diffraction pattern of the single crystal structure (SC_RT) determined at room temperature is similar to the PXRD pattern at 296 K (RT). At 380 K, the peak at 6.45° starts to disappear, while the peak at 6° shifts toward lower angles, indicative of changes in the unit cell parameters. Also, the characteristic peak of the desolvated phase emerges at 6.7°, signifying the formation of the distinct phase. At 395 K, the phase transformation is complete, and the PXRD patterns closely resemble the 2:1 desolvated structure (SC_HT). This closely matches the observed temperatures in DSC and TGA. The difference in reported desolvation temperatures can be attributed to the absence of carrier gas in the case of the VT-PXRD performed within a closed capillary.

Preprints (www.preprints.org) | NOT PEER-REVIEWED | Posted: 8 January 2024 doi:10.20944/preprints202401.0598.v1



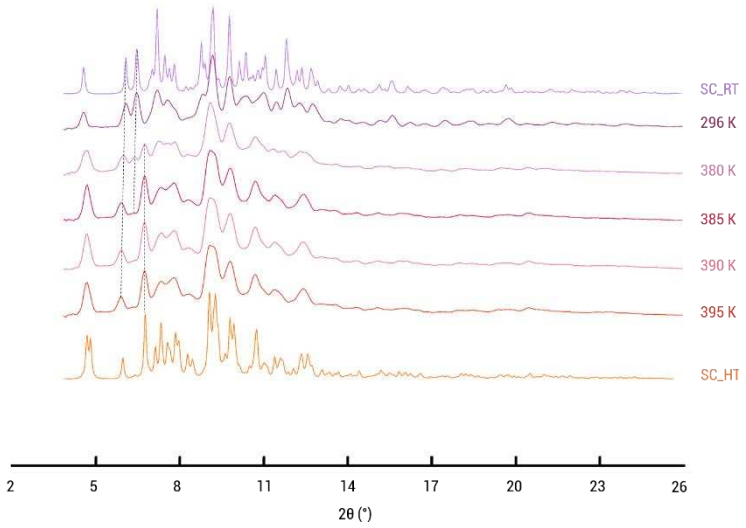


**Figure 9.** Variable-temperature X-ray powder diffraction patterns of PZQ-CU-EtOAc (2:1:1) cocrystal solvate. The temperature range is from 296 K to 395 K.

## 4. Conclusions

In this study, we investigated the cocrystallization potential between praziquantel (PZQ) and curcumin (CU), allowing us to identify two new solid forms: a GRAS cocrystal solvate and a non-solvated cocrystal. Here, we have successfully highlighted the potential of crystal engineering to combine a drug and a nutraceutical.

Further investigation and experiment, such as single crystal analysis, confirmed the formation of a praziquantel-curcumin-ethyl acetate (2:1:1) cocrystal solvate as well as a praziquantel-curcumin (2:1) cocrystal, obtained by solvent loss. Upon heating, the cocrystal solvate loses ethyl acetate molecules occupying voids with minimal interaction within the crystal lattice, and the transition to a non-solvated cocrystal occurs. Comparing the solvate and non-solvate structures, only subtle differences in solid-state arrangements occur.

Thermal analyses revealed that the cocrystal solvate remains stable up to approximately 100°C, at which point a transition to the non-solvated phase occurs. This latter melts at 130°C, which is a lower melting point compared to the individual components.

VT-XRPD experiments, conducted over the temperature range from RT to 395 K, elucidated the thermal behaviors and phase transition from the (2:1:1) cocrystal solvate to the desolvated (2:1) cocrystal. The close alignment of the results with temperatures observed in DSC and TGA emphasizes the importance of experimental conditions, particularly the absence of carrier gas in VT-XRPD conducted within a closed capillary.

Exploring the impact of curcumin on the bitterness of praziquantel, as well as its potential mitigating effects on the adverse reactions associated with the drug in the cocrystal, would be of scientific interest for future applications.

In conclusion, we here showcase a new praziquantel-nutraceutical cocrystal, which furthermore can be obtained as a stable GRAS solvate cocrystal, with potential implications for pharmaceutical applications.

**Supplementary Materials:** The following are available online at www.mdpi.com/xxx/s1, Figure S1: title, Table S1: title, Video S1: title.

**Author Contributions:** The manuscript was written through contributions of all authors. All authors have given approval to the final version of the manuscript.

**Funding:** This work has been funded by Actions de Recherche Concerté (ARC) under the project PURE- 20/25-108 - New approaches in Process Intensification: Towards combined PUrefication-REaction Membrane based processes and by the Fonds de la Recherche Scientifique (FNRS) CDR J.0168.22.

**Data Availability Statement:**

**Acknowledgments:** This work has been funded by Actions de Recherche Concerté (ARC) under the project PURE- 20/25-108 - New approaches in Process Intensification: Towards combined PUrefication-REaction Membrane based processes.

**Conflicts of Interest:**

## References

1. McManus, D. P.; Dunne, D. W.; Sacko, M.; Utzinger, J.; Vennervald, B. J.; Zhou, X.-N. Schistosomiasis. Nat Rev Dis Primers 2018, 4 (1), 1–19. https://doi.org/10.1038/s41572-018-0013-8
2. Colley, D. G.; Bustinduy, A. L.; Secor, W. E.; King, C. H. Human Schistosomiasis. Lancet 2014, 383 (9936), 2253–2264. https://doi.org/10.1016/S0140-6736(13)61949-2
3. Kokaliaris, C.; Garba, A.; Matuska, M.; Bronzan, R. N.; Colley, D. G.; Dorkenoo, A. M.; Ekpo, U. F.; Fleming, F. M.; French, M. D.; Kabore, A.; Mbonigaba, J. B.; Midzi, N.; Mwinzi, P. N. M.; N'Goran, E. K.; Polo, M. R.; Sacko, M.; Tchuem Tchuenté, L.-A.; Tukahebwa, E. M.; Uvon, P. A.; Yang, G.; Wiesner, L.; Zhang, Y.; Utzinger, J.; Vounatsou, P. Effect of Preventive Chemotherapy with Praziquantel on Schistosomiasis among School-Aged Children in Sub-Saharan Africa: A Spatiotemporal Modelling Study. The Lancet Infectious Diseases 2022, 22 (1), 136–149. https://doi.org/10.1016/S1473-3099(21)00090-6
4. Schistosomiasis. https://www.who.int/news-room/fact-sheets/detail/schistosomiasis (accessed 2023-10-23)
5. WHO Model Lists of Essential Medicines. https://www.who.int/groups/expert-committee-on-selection-and-use-of-essential-medicines/essential-medicines-lists (accessed 2023-07-05)
6. Borrego-Sánchez, A.; Viseras, C.; Aguzzi, C.; Sainz-Díaz, C. I. Molecular and Crystal Structure of Praziquantel. Spectroscopic Properties and Crystal Polymorphism. European Journal of Pharmaceutical Sciences 2016, 92, 266–275. https://doi.org/10.1016/j.ejps.2016.04.023
7. Meyer, T.; Sekljic, H.; Fuchs, S.; Bothe, H.; Schollmeyer, D.; Miculka, C. Taste, A New Incentive to Switch to (R)-Praziquantel in Schistosomiasis Treatment. PLoS Negl Trop Dis 2009, 3 (1), e357. https://doi.org/10.1371/journal.pntd.0000357
8. Cappuccino, C.; Spoletti, E.; Renni, F.; Muntoni, E.; Keiser, J.; Voinovich, D.; Perissutti, B.; Lusi, M. Co-Crystalline Solid Solution Affords a High-Soluble and Fast-Absorbing Form of Praziquantel. Mol. Pharmaceutics 2023, 20 (4), 2009–2016. https://doi.org/10.1021/acs.molpharmaceut.2c00984
9. Navaratnam, A. M. D.; Sousa-Figueiredo, J. C.; Stothard, J. R.; Kabatereine, N. B.; Fenwick, A.; Mutumba-Nakalembe, M. J. Efficacy of Praziquantel Syrup versus Crushed Praziquantel Tablets in the Treatment of Intestinal Schistosomiasis in Ugandan Preschool Children, with Observation on Compliance and Safety. Trans R Soc Trop Med Hyg 2012, 106 (7), 400–407. https://doi.org/10.1016/j.trstmh.2012.03.013
10. Babu, N. J.; Nangia, A. Solubility Advantage of Amorphous Drugs and Pharmaceutical Cocrystals. Crystal Growth & Design 2011, 11 (7), 2662–2679. https://doi.org/10.1021/cg200492w
11. Bernstein, J. Polymorphism of Pharmaceuticals. In Polymorphism in Molecular Crystals, 1st ed.; Oxford University Press: New York, 2002; pp 240-255.
12. Serajuddin, A. T. M. Salt Formation to Improve Drug Solubility. Advanced Drug Delivery Reviews 2007, 59 (7), 603–616. https://doi.org/10.1016/j.addr.2007.05.010
13. Good, D. J.; Rodríguez-Hornedo, N. Solubility Advantage of Pharmaceutical Cocrystals. Crystal Growth & Design 2009, 9 (5), 2252–2264. https://doi.org/10.1021/cg801039j
14. Espinosa-Lara, J. C.; Guzman-Villanueva, D.; Arenas-García, J. I.; Herrera-Ruiz, D.; Rivera-Islas, J.; Román-Bravo, P.; Morales-Rojas, H.; Höpfl, H. Cocrystals of Active Pharmaceutical Ingredients—Praziquantel in Combination with Oxalic, Malonic, Succinic, Maleic, Fumaric, Glutaric, Adipic, And Pimelic Acids. Crystal Growth & Design 2013, 13 (1), 169–185. https://doi.org/10.1021/cg301314w
15. Zanolla, D.; Perissutti, B.; Passerini, N.; Chierotti, M. R.; Hasa, D.; Voinovich, D.; Gigli, L.; Demitri, N.; Geremia, S.; Keiser, J.; Cerreia Vioglio, P.; Albertini, B. A New Soluble and Bioactive Polymorph of Praziquantel. European Journal of Pharmaceutics and Biopharmaceutics 2018, 127, 19–28. https://doi.org/10.1016/j.ejpb.2018.01.018
16. Zanolla, D.; Perissutti, B.; Vioglio, P. C.; Chierotti, M. R.; Gigli, L.; Demitri, N.; Passerini, N.; Albertini, B.; Franceschinis, E.; Keiser, J.; Voinovich, D. Exploring Mechanochemical Parameters Using a DoE Approach: Crystal Structure Solution from Synchrotron XRPD and Characterization of a New Praziquantel Polymorph. European Journal of Pharmaceutical Sciences 2019, 140, 105084. https://doi.org/10.1016/j.ejps.2019.105084
17. Zanolla, D.; Hasa, D.; Arhangelskis, M.; Schneider-Rauber, G.; Chierotti, M. R.; Keiser, J.; Voinovich, D.; Jones, W.; Perissutti, B. Mechanochemical Formation of Racemic Praziquantel Hemihydrate with Improved Biopharmaceutical Properties. Pharmaceutics 2020, 12 (3), 289. https://doi.org/10.3390/pharmaceutics12030289

18. Zanolla, D.; Gigli, L.; Hasa, D.; Chierotti, M. R.; Arhangelskis, M.; Demitri, N.; Jones, W.; Voinovich, D.; Perissutti, B. Mechanochemical Synthesis and Physicochemical Characterization of Previously Unreported Praziquantel Solvates with 2-Pyrrolidone and Acetic Acid. Pharmaceutics 2021, 13 (10), 1606. https://doi.org/10.3390/pharmaceutics13101606
19. Sánchez-Guadarrama, O.; Mendoza-Navarro, F.; Cedillo-Cruz, A.; Jung-Cook, H.; Arenas-García, J. I.; Delgado-Díaz, A.; Herrera-Ruiz, D.; Morales-Rojas, H.; Höpfl, H. Chiral Resolution of RS-Praziquantel via Diastereomeric Co-Crystal Pair Formation with l-Malic Acid. Crystal Growth & Design 2016, 16 (1), 307–314. https://doi.org/10.1021/acs.cgd.5b01254
20. Devogelaer, J.-J.; Charpentier, M. D.; Tijink, A.; Dupray, V.; Coquerel, G.; Johnston, K.; Meekes, H.; Tinnemans, P.; Vlieg, E.; Ter Horst, J. H.; De Gelder, R. Cocrystals of Praziquantel: Discovery by Network-Based Link Prediction. Crystal Growth & Design 2021, 21 (6), 3428–3437. https://doi.org/10.1021/acs.cgd.1c00211
21. Yang, D.; Cao, J.; Heng, T.; Xing, C.; Yang, S.; Zhang, L.; Lu, Y.; Du, G. Theoretical Calculation and Structural Analysis of the Cocrystals of Three Flavonols with Praziquantel. Crystal Growth & Design 2021, 21 (4), 2292–2300. https://doi.org/10.1021/acs.cgd.0c01706
22. Liu, Q.; Yang, D.; Chen, T.; Zhang, B.; Xing, C.; Zhang, L.; Lu, Y.; Du, G. Insights into the Solubility and Structural Features of Four Praziquantel Cocrystals. Crystal Growth & Design 2021, 21 (11), 6321–6331. https://doi.org/10.1021/acs.cgd.1c00785
23. Rodríguez-Ruiz, C.; Salas-Zúñiga, R.; Sánchez-Guadarrama, M. O.; Delgado-Díaz, A.; Herrera-Ruiz, D.; Morales-Rojas, H.; Höpfl, H. Structural, Physicochemical, and Biopharmaceutical Properties of Cocrystals with RS - and R -Praziquantel─Generation and Prolongation of the Supersaturation State in the Presence of Cellulosic Polymers. Crystal Growth & Design 2022, 22 (10), 6023–6038. https://doi.org/10.1021/acs.cgd.2c00661
24. Yang, S.; Liu, Q.; Ji, W.; An, Q.; Song, J.; Xing, C.; Yang, D.; Zhang, L.; Lu, Y.; Du, G. Cocrystals of Praziquantel with Phenolic Acids: Discovery, Characterization, and Evaluation. Molecules 2022, 27 (6), 2022. https://doi.org/10.3390/molecules27062022
25. Esatbeyoglu, T.; Huebbe, P.; Ernst, I. M. A.; Chin, D.; Wagner, A. E.; Rimbach, G. Curcumin—From Molecule to Biological Function. Angewandte Chemie International Edition 2012, 51 (22), 5308–5332. https://doi.org/10.1002/anie.201107724
26. Kotha, R. R.; Luthria, D. L. Curcumin: Biological, Pharmaceutical, Nutraceutical, and Analytical Aspects. Molecules 2019, 24 (16), 2930. https://doi.org/10.3390/molecules24162930
27. Kharat, M.; Du, Z.; Zhang, G.; McClements, D. J. Physical and Chemical Stability of Curcumin in Aqueous Solutions and Emulsions: Impact of PH, Temperature, and Molecular Environment. J. Agric. Food Chem. 2017, 65 (8), 1525–1532. https://doi.org/10.1021/acs.jafc.6b04815
28. Kunnumakkara, A. B.; Bordoloi, D.; Padmavathi, G.; Monisha, J.; Roy, N. K.; Prasad, S.; Aggarwal, B. B. Curcumin, the Golden Nutraceutical: Multitargeting for Multiple Chronic Diseases. British journal of pharmacology 2017, 174 (11), 1325–1348. https://doi.org/10.1111/bph.13621
29. Sharifi-Rad, J.; Rayess, Y. E.; Rizk, A. A.; Sadaka, C.; Zgheib, R.; Zam, W.; Sestito, S.; Rapposelli, S.; Neffe-Skocińska, K.; Zielińska, D.; Salehi, B.; Setzer, W. N.; Dosoky, N. S.; Taheri, Y.; El Beyrouthy, M.; Martorell, M.; Ostrander, E. A.; Suleria, H. A. R.; Cho, W. C.; Maroyi, A.; Martins, N. Turmeric and Its Major Compound Curcumin on Health: Bioactive Effects and Safety Profiles for Food, Pharmaceutical, Biotechnological and Medicinal Applications. Front Pharmacol 2020, 11, 01021. https://doi.org/10.3389/fphar.2020.01021
30. Canistro, D.; Chiavaroli, A.; Cicia, D.; Cimino, F.; Curro, D.; Dell'Agli, M.; Ferrante, C.; Giovannelli, L.; Leone, S.; Martinelli, G. The Pharmacological Basis of the Curcumin Nutraceutical Uses: An Update. Pharmadvances 2021, 3 (2), 421–466. https://dx.doi.org/10.36118/pharmadvances.2021.06
31. Tabanelli, R.; Brogi, S.; Calderone, V. Improving Curcumin Bioavailability: Current Strategies and Future Perspectives. Pharmaceutics 2021, 13 (10), 1715. https://doi.org/10.3390/pharmaceutics13101715.
32. Sanphui, P.; Goud, N. R.; Khandavilli, U. R.; Nangia, A. Fast Dissolving Curcumin Cocrystals. Crystal Growth & Design 2011, 11 (9), 4135–4145. https://doi.org/10.1021/cg200704s
33. Rathi, N.; Paradkar, A.; Gaikar, V. G. Polymorphs of Curcumin and Its Cocrystals With Cinnamic Acid. Journal of Pharmaceutical Sciences 2019, 108 (8), 2505–2516. https://doi.org/10.1016/j.xphs.2019.03.014
34. Dal Magro, C.; dos Santos, A. E.; Ribas, M. M.; Aguiar, G. P. S.; Volfe, C. R. B.; Lopes, M. L. L. C.; Siebel, A. M.; Müller, L. G.; Bortoluzzi, A. J.; Lanza, M.; Oliveira, J. V. Production of Curcumin-Resveratrol Cocrystal Using Cocrystallization with Supercritical Solvent. The Journal of Supercritical Fluids 2021, 171, 105190. https://doi.org/10.1016/j.supflu.2021.105190
35. Sathisaran, I.; Dalvi, S. V. Crystal Engineering of Curcumin with Salicylic Acid and Hydroxyquinol as Coformers. Crystal Growth & Design 2017, 17 (7), 3974–3988. https://doi.org/10.1021/acs.cgd.7b00599
36. Thakuria, R.; Sarma, B. Drug-Drug and Drug-Nutraceutical Cocrystal/Salt as Alternative Medicine for Combination Therapy: A Crystal Engineering Approach. Crystals 2018, 8 (2), 101. https://doi.org/10.3390/cryst8020101

37. Sinha, A. S.; Maguire, A. R.; Lawrence, S. E. Cocrystallization of Nutraceuticals. Crystal Growth & Design 2015, 15 (2), 984–1009. https://doi.org/10.1021/cg501009c
38. Macrae, C.F.; Sovago, I.; Cottrell, S.J.; Galek, P.T.A; McCabe, P.; Pidcock, E.; Platings, M; Shields, G.P.; Stevens, J.S.; Towler, M.; et al. Mercury 4.0: From Visualization to Analysis, Design and Prediction. J. Appl. Cryst. 2020, 56, 226-235. https://doi.org/10.1107/S1600576719014092
39. Roisnel, T.; Rodríquez-Carvajal, J. WinPLOTR: A Windows Tool for Powder Diffraction Pattern Analysis. Materials Science Forum 2001, 378–381, 118–123. https://doi.org/10.4028/www.scientific.net/MSF.378-381.118
40. Rigaku Oxford Diffraction. CrysalisPro Software System, Version 1.171.38.41l.; Rigaku Oxford Diffraction Ltd.: Oxford, UK, 2015.
41. Sheldrick, G.M. XS, version 2013/1; Georg-August-Universität Göttingen: Göttingen, Germany. Sheldrick, G. M. SHELXT – Integrated Space-Group and Crystal-Structure Determination. Acta Cryst A 2015, 71 (1), 3–8. https://doi.org/10.1107/S2053273314026370
42. Sheldrick, G. M. Crystal Structure Refinement with SHELXL. Acta Cryst C 2015, 71 (1), 3–8. https://doi.org/10.1107/S2053229614024218
43. Spek, A. L. Structure Validation in Chemical Crystallography. Acta Cryst D 2009, 65 (2), 148–155. https://doi.org/10.1107/S090744490804362X
44. Etter, M.C. Encoding and Decoding Hydrogen-Bond Patterns of Organic Compounds. Acc. Chem. Res. 1990, 23, 120–126. https://doi.org/10.1021/ar00172a005